Article

EGDMA- and TRIM-Based Microparticles Imprinted with 5-Fluorouracil for Prolonged Drug Delivery

Michał Cegłowski [1,*], **Joanna Kurczewska** [1], **Aleksandra Lusina** [1], **Tomasz Nazim** [1] **and Piotr Ruszkowski** [2]

[1] Faculty of Chemistry, Adam Mickiewicz University, 61-614 Poznan, Poland; asiaw@amu.edu.pl (J.K.); aleksandra.lusina@amu.edu.pl (A.L.); tomasz.nazim@amu.edu.pl (T.N.)

[2] Department of Pharmacology, Poznan University of Medical Sciences, 61-614 Poznan, Poland; pruszkowski@gmail.com

[*] Correspondence: michal.ceglowski@amu.edu.pl; Tel.: +48-61-8291-799

Abstract: Imprinted materials possess designed cavities capable of forming selective interactions with molecules used in the imprinting process. In this work, we report the synthesis of 5-fluorouracil (5-FU)-imprinted microparticles and their application in prolonged drug delivery. The materials were synthesized using either ethylene glycol dimethacrylate (EGDMA) or trimethylolpropane trimethacrylate (TRIM) cross-linkers. For both types of polymers, methacrylic acid was used as a functional monomer, whereas 2-hydroxyethyl methacrylate was applied to increase the final materials' hydrophilicity. Adsorption isotherms and adsorption kinetics were investigated to characterize the interactions that occur between the materials and 5-FU. The microparticles synthesized using the TRIM cross-linker showed higher adsorption properties towards 5-FU than those with EGDMA. The release kinetics was highly dependent upon the cross-linker and pH of the release medium. The highest cumulative release was obtained for TRIM-based microparticles at pH 7.4. The IC_{50} values proved that 5-FU-loaded TRIM-based microparticles possess cytotoxic activity against HeLa cell lines similar to pure 5-FU, whereas their toxicity towards normal HDF cell lines was ca. three times lower than for 5-FU.

Keywords: molecularly imprinted polymers; microspheres; drug delivery; 5-fluorouracil

1. Introduction

Drug delivery systems (DDS) are sophisticated technologies that allow targeted delivery of particular pharmaceutical or controlled therapeutic agents' release. DDS application is essential for therapeutic agents limited due to their low solubility, drug administration issues, or very fast metabolism. Moreover, the application of DDS allows to optimize drug efficiency and improve administration, while lowering the possibility of causing adverse side effects. As a result, the development of new DDS occurs in parallel with creating new therapeutic agents. Whenever a new drug has a limited therapeutic effect in a free form, the combination of drugs and DDS may overcome this problem. The design, synthesis, and production of new substances and materials that can be applied to prepare new DDS have become a major topic of many research groups. Their goal is to develop a DDS which would allow drug administration to a specific site with a known quantity and for a precise amount of time. It is, of course, necessary to produce DDS that, as well as their metabolites, show no toxicity and are easily removed from the human body [1–3].

Various materials have been used to generate DDS. The most frequently used are lipids [4,5], chitosan [6,7], silica [8–10], halloysite [11,12], functional polymers [13–19], and dendrimers [20,21]. Among the described materials, functional polymers are frequently used due to their high synthetic versatility, a broad range of final properties, and various possible applications [22,23]. Sophisticated polymeric DDS should guarantee drug delivery

in a predesigned manner. Functional polymers can be designed to fulfill the most sophisticated criteria of DDS. They can be synthesized to become triggered-release DDS or release a drug following a particular kinetic profile. As a result, it is possible to obtain passive or active targeting, which means that the whole system is responsible for the therapeutic benefit. Molecularly imprinted polymers (MIPs) represent a group of functional polymers that can be easily tuned to possess a defined affinity to a drug molecule, and thus they often find application in producing new DDS [24–26].

MIPs are synthesized by copolymerizing a cross-linker mixed with a complex formed by functional monomers and template molecules. The cross-linker initiates the formation of the bulk polymer structure and entrapment of the template molecules inside, whereas functional monomers form stable, non-covalent interactions with template molecules. Finally, it results in the synthesis of MIPs selective towards the template used, which can be reversibly bound by cavities formed during the reaction. As a result, they have found many applications in fields such as solid-phase extraction (SPE) [27–29], development of sensors [30–32], and drug delivery [33,34].

Many researchers find the application of MIPs in drug delivery particularly interesting due to the possibility of producing materials that alter their interaction strength with drug molecules influenced by a specific change in the environment. MIPs possess an enhanced affinity to the drug template, which increases the residence time of the drug. Moreover, MIPs' properties allow for reaching high drug loading, and the fact that the drug is entrapped within the polymeric network results in its higher stability and durability against harsh conditions. MIPs can be synthesized as smart materials that can be effectively used to produce DDS, considering that they can be programmed to release therapeutic agents as a response to defined stimuli [35]. MIPs can also be synthesized to develop materials that release molecules entrapped inside cavities with a particular kinetic profile [36]. This can be achieved by selecting the appropriate type and amount of functional monomers present in the MIPs' structure. Our group recently published a detailed investigation about using MIPs for prolonged drug delivery of doxorubicin [37] and paclitaxel [38].

MIPs are synthesized as monoliths that are ground to obtain particles of desired dimensions for numerous applications. Although this process is frequently used in analytical applications such as SPE, the development of DDS requires more rigorous control over polymer particles' size. New synthetic methods that allow obtaining MIPs as uniform nanoparticles or microparticles have been developed to solve this problem. As synthesized materials possess a significantly increased surface area, more cavities are closer to the surface, making them easily accessible. The additional benefit of small particle sizes is their ability to form stable dispersions in various solvents, which increases their attractiveness as potential materials to be used as DDS [39–41].

In this work, we report the synthesis and characterization of MIPs microparticles imprinted with 5-fluorouracil (5-FU). 5-FU is a cytotoxic drug with a broad activity spectrum against numerous tumors. It undergoes fast metabolism in the human body, and thus a therapy consisting of high doses is required, which can cause severe toxic effects in many patients [42]. As a result, new DDS for 5-FU are being developed [43]. The advantage of using microparticles for drug delivery is that they do not traverse into the interstitium over the size of 100 nm transported by the lymph, and thus they only act locally in a place of administration [44]. Methacrylate-based particulate carriers are widely applied for biomedical applications to obtain drug delivery systems. The therapeutic agent's release from their structure typically occurs in a biphasic way with an incomplete drug release. The release mechanism can be described using both Fickian and non-Fickian kinetic models. The improvement of drug release can be achieved by increasing polymer hydrophilicity by synthesizing functional microspheres with additional functional groups or formulating composites with hydrophilic polymers [45]. The microparticles were synthesized by using precipitation polymerization. Methacrylic acid (MAA) was used as a functional monomer, whereas 2-hydroxyethyl methacrylate (HEMA) was used as a hydrophilic monomer to improve the water compatibility of the final materials. The microparticles were prepared using

two cross-linkers, particularly ethylene glycol dimethacrylate (EGDMA) and trimethylol-propane trimethacrylate (TRIM), to examine the influence of the polymer matrix structure on the final properties of microparticles. The interactions of MIPs with 5-FU were investigated by examining their adsorption properties and release profiles of 5-FU. Finally, the in vitro activity of 5-FU-loaded MIPs against HeLa, U87 MG, A-549, KB, and MCF-7 cancer cell lines was investigated. The results were compared with the measurements performed against human dermal fibroblasts (HDF) normal cell lines. To the best of our knowledge, this is the first research describing the synthesis of 5-FU-imprinted hydrophilic microparticles and presenting their in vitro activity against cancer and normal cell lines.

2. Materials and Methods

2.1. Materials and Chemicals

Ethylene glycol dimethacrylate, methacrylic acid, trimethylolpropane trimethacrylate, 2-hydroxyethyl methacrylate, 5-fluorouracil, 2,2′-azobisisobutyronitrile solution (AIBN; 0.2 M in toluene), and all solvents (HPLC grade) were obtained from Sigma-Aldrich (St. Louis, MO, USA).

2.2. Instruments

The FTIR measurements were performed using a IFS 66/s spectrometer (Bruker, Billerica, MA, USA). To obtain spectra, 1.5 mg of each material was mixed with ca. 200 mg of KBr, and the resulting powder was converted into tablets used in FTIR measurements. Thermogravimetric (TG) analysis was performed using a Setsys 1200 (Setaram, Caluire, France) apparatus. The analysis was performed in an air stream (50 mL min^{-1}) at a heating rate of 10 °C min^{-1}. Scanning electron microscopy (SEM) images were recorded using a Scanning Electron Microscope SU3500 (Hitachi, Tokyo, Japan). UV-Vis absorption spectra were obtained using a 8453 (Agilent, Santa Clara, CA, USA) spectrophotometer. The solutions' pH values were controlled with an CP-505 pH meter (Elmetron, Zabrze, Poland).

2.3. Synthesis of Microparticles

MIPs created using EGDMA cross-linker were synthesized as follows. The pre-polymerization mixture consisting of 5-FU (0.9 mmol), MAA (1.8 mmol), HEMA (0.9 mmol), and methanol (90 mL) was prepared in a glass pressure tube. The mixture was degassed for 30 min using an ultrasound bath and purging with inert gas (nitrogen). Subsequently, EGDMA (8 mmol) and AIBN solutions (1 mL) were added, and the tube was degassed for an additional 10 min. Afterward, the tube was sealed and placed at 60 °C for 18 h. As-synthesized microparticles were filtered off and dried under a vacuum. The resulting drug-loaded MIPs were placed in a dialysis tubing to remove template molecules and were dialyzed against acidified methanol (9:1 methanol/acetic acid). This process was continued until 5-FU was no longer detected in a dialysis solution. The drug-unloaded MIPs cross-linked with EGDMA (denoted as MIP$_{EGDMA}$) were finally dried under a vacuum.

MIPs created using the TRIM cross-linker were prepared by the same setup and procedure as EGDMA-based MIPs, but with different amounts of reagents. The polymerization mixture consisted of 5-FU (2 mmol), MAA (4 mmol), HEMA (2 mmol), and methanol (80 mL). After degassing and sonication, TRIM (4 mmol) and AIBN solutions (1.4 mL) were added, and the tube was degassed for an additional 10 min. The remaining procedure is identical to EGDMA-based MIPs. Finally, the drug-unloaded MIPs cross-linked with TRIM were denoted as MIP$_{TRIM}$.

The corresponding non-imprinted polymers (NIPs) were synthesized using analogous procedures but without adding template molecules. The obtained microparticles were denoted as NIP$_{EGDMA}$ and NIP$_{TRIM}$. The structures of all used monomers and templates are presented in Figure S1.

2.4. Adsorption Studies

Adsorption isotherms were established using batch experiments, in which 10 mL of methanolic 5-FU solution at concentrations ranging from 0.39 to 50 mg L^{-1} was added to 10 mg of MIPs or NIPs. The obtained mixtures were equilibrated for 24 h at ambient conditions (25 °C). UV-vis absorption spectra were taken prior to and after adsorption solutions to establish the concentration of 5-FU. The amount of adsorbed 5-FU (q_{eq}, mg g^{-1}) was calculated as follows:

$$q_{eq} = \frac{(C_0 - C_{eq})V}{m} \tag{1}$$

where C_0 is the initial concentration of 5-FU solution (mg mL^{-1}), C_{eq} is the equilibrium concentration of 5-FU solution (mg mL^{-1}), m is the polymer (MIPs/NIPs) mass (g), and V is the volume of 5-FU solution (mL). The experiments were repeated three times, and mean values were used for calculation.

The adsorption kinetics studies were conducted when 50 mg of either MIPs or NIPs were placed in 50 mL of 5-FU solution in methanol with an initial concentration of 10 mg L^{-1}. The solution was stirred at ambient conditions, and the concentration of 5-FU was measured at defined time intervals by UV-vis absorption spectra. The q_t value (mg g^{-1}), which represents the amount of adsorbed 5-FU, was calculated as follows:

$$q_t = \frac{(C_0 - C_t)V}{m} \tag{2}$$

where C_t is the concentration of 5-FU after time t (h).

2.5. Release Experiments

The dissolution method was used to conduct the in vitro release studies. The experiments were conducted by dispersing 5-FU-loaded MIPs (20 mg) in buffer solutions (10 mL) at pH 2.2, 5.0, and 7.4. The solutions were stirred continuously for seven days at 37 °C, and at specified time intervals, the samples were collected, centrifuged, and their UV-vis absorption spectra were recorded. The obtained data allowed to calculate the amount of drug releases from studied MIPs. The experiments were repeated three times, and the obtained mean values were used for subsequent calculations.

The results obtained for the 5-FU release were fitted using various models that characterize the mechanism of the release process. The following models were applied: zero-order (Equation (3)), first-order (Equation (4)), simplified Higuchi (Equation (5)), Hixson–Crowell (Equation (6)), and Korsmeyer–Peppas (Equation (7)). The following equations mathematically represent these models:

$$F_t = k_0 t \tag{3}$$

$$F_t = 1 - e^{-k_1 t} \tag{4}$$

$$F_t = k_H \sqrt{t} \tag{5}$$

$$\sqrt[3]{F_0} - \sqrt[3]{F_t} = k_{HC} t \tag{6}$$

$$F_t = k_{KP} t^n \tag{7}$$

where F_t is the amount of 5-FU released at a specified time "t", F_0 is the initial amount of 5-FU in MIPs structure, k_0, k_1, k_H, k_{HC}, and k_{KP} are the release constants of corresponding equations, and n is the diffusion exponent.

2.6. Cytotoxicity Assays

The cytotoxicity assays were performed using the experimental procedure described in our previous research. Briefly, KB, HeLa, and MCF-7 cell lines were obtained from The European Collection of Cell Cultures (ECACC) supplied by Sigma-Aldrich (St. Louis, MO, USA). whereas A-549, U-87MG, and HDF cell lines were purchased from the American Type Cell Collection (ATCC) through LGC Standards. Approximately 0.1 mL of the diluted

cell suspension (ca. 10,000 cells) was added to every well of the microtiter plate. A partial monolayer was formed after 24 h, and the supernatant was washed out. Then, 100 μL of 6 different 5-FU concentrations (0.1, 0.2, 1, 2, 10, and 20 μM) or number of MIPs that release the corresponding amount of 5-FU were added to the cells in microtiter plates. For NIPs blank experiments, the same mass of microparticles was used as for MIPs. Other experimental details were described in our previous work.

2.7. Statistical Analysis

One-way ANOVA with the post-hoc Tukey HSD test was used to test statistical significance. A *p*-value lower than 0.05 was considered as statistically significant.

3. Results and Discussion

The synthesized imprinted microparticles and corresponding non-imprinted microparticles present similar bands in the IR spectra (Figures S2 and S3), which indicates that the polymeric materials' main structure for all samples is similar. For all synthesized materials, the stretching and bending O-H vibrations of carboxyl groups originating from MAA can be observed at 3562 and 1389 cm^{-1}, respectively. These bands overlap with O-H stretching, and bending vibrations originated from hydroxyl groups of HEMA. The asymmetric stretching vibrations of CH_2 groups can be observed at 2955 cm^{-1} for EGDMA-based microparticles and 2974 for TRIM-based microparticles. The stretching vibrations of C=O bonds are observed at 1730 cm^{-1} for EGDMA-based microparticles and 1734 cm^{-1} for TRIM-based microparticles. The symmetric and asymmetric C-O stretching vibrations of ester groups can be observed at 1258 and 1161 cm^{-1} for EGDMA-based microparticles, respectively. For TRIM-based microparticles, these signals are observed at 1268 and 1156 cm^{-1}, respectively [46,47]. Drug-loaded MIP_{EGDMA} shows a band characteristic for 5-FU at 816 cm^{-1}, whereas for drug-loaded MIP_{TRIM}, these additional bands can be observed at 816, 553, and 471 cm^{-1}.

SEM images of EGDMA- and TRIM-based microparticles are presented in Figure 1. For drug-loaded and drug-unloaded MIPs microparticles, no differences in SEM images were observed. SEM images of NIP_{EGDMA} present microparticles of 0.7–1.3 μm in diameter, whereas MIP_{EGDMA} microparticles are much smaller, ranging between 300 and 600 nm. This result clearly indicates that the presence of 5-FU in the polymerization mixture results in the formation of smaller microparticles. The NIP_{TRIM} microparticles are also smaller than those synthesized using EGDMA as a cross-linker, and their size ranges between 400 and 800 nm. Contrary to the previous observation, the presence of 5-FU in the polymerization mixture has not influenced the size of MIP_{TRIM} microparticles. This result may indicate that the presence of three methacrylate groups in the cross-linker structure that undergo polymerization makes the process less prone to the presence of additional substances in the reaction mixture that can affect the reaction.

The TG results obtained for EGDMA-based microparticles are presented in Figure S4, whereas those obtained for TRIM-based microparticles are shown in Figure S5. All EGDMA-based microparticles demonstrate one major decomposition step, from ca. 200 to ca. 450 °C. This step refers to the polymer structure's decomposition and results in almost complete oxidation of organic material. For 5-FU-loaded MIP_{EGDMA} microparticles, an increased weight loss is observed in the initial decomposition step compared to drug-unloaded material. It probably results from the decomposition of 5-FU molecules. Compared to EGDMA-based microparticles, all TRIM-based microparticles are characterized by only one major decomposition step, that starts at around 300 °C and ends at around 475 °C, reflecting almost complete oxidation of the polymer material. For 5-FU-loaded MIP_{TRIM}, only a slight increase in the weight loss of the initial decomposition step is observed compared with drug-unloaded material, which is connected with the decomposition of 5-FU molecules. The increase in the weight loss occurs within the 260–320 °C range, which is in accordance with the decomposition temperature of 5-FU reported in the literature [48].

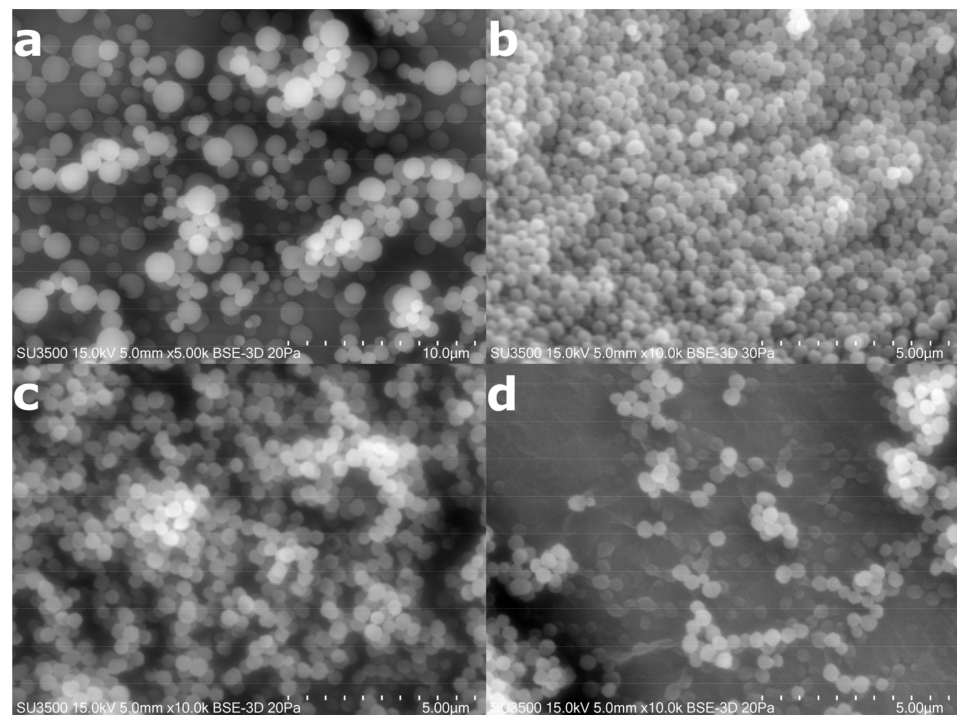**Figure 1.** SEM images of (**a**) NIP_{EGDMA}, (**b**) MIP_{EGDMA}, (**c**) NIP_{TRIM}, and (**d**) MIP_{TRIM}.

3.1. Adsorption Isotherms

The adsorption process's characterization is achieved by plotting adsorption isotherms for experimental data obtained during adsorption of 5-FU by the microparticles at the equilibrium state. Figure 2 shows the relationship between the 5-FU equilibrium concentration and the amount of 5-FU adsorbed by 1 g of the appropriate adsorbent. To characterize the experimental data, Langmuir and Freundlich adsorption isotherm models were used for interpretation.
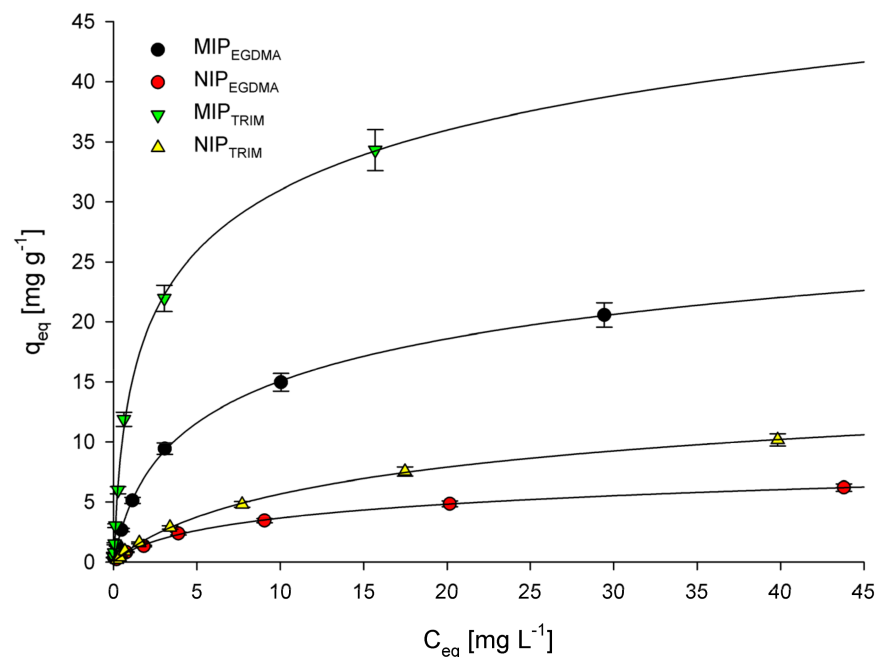

Figure 2. Adsorption isotherms of 5-FU onto MIP_{EGDMA}, NIP_{EGDMA}, MIP_{TRIM}, and NIP_{TRIM}.

The following equation represents the Langmuir adsorption isotherm:

$$\frac{C_{eq}}{q_{eq}} = \frac{C_{eq}}{q_m} + \frac{1}{Kq_m} \tag{8}$$

where K (L mg^{-1}) is the binding equilibrium constant, q_m (mg g^{-1}) is the maximum amount of bonded 5-FU, C_{eq} (mg L^{-1}) is the equilibrium concentration of 5-FU, and q_{eq} (mg g^{-1}) is the amount of 5-FU adsorbed at the equilibrium concentration. Table 1 summarizes the values of K, qm, and R^2 (correlation coefficients). The R^2 values obtained for all synthesized microparticles are high (above 0.98), indicating that the Langmuir adsorption model nicely fits the experimental data. The confirmation of successful imprinting can be found in the high difference between the maximum adsorption capacity (q_m) between MIPs and corresponding to them NIPs. For both MIPs–NIPs pairs, the q_m value is around three times higher in favor of MIPs. There is also a significant difference in q_m values between the corresponding materials synthesized using different cross-linkers. The calculated data clearly show that the maximum adsorption capacity values are higher for MIP$_{TRIM}$ and NIP$_{TRIM}$ than for MIP$_{EGDMA}$ and NIP$_{EGDMA}$, respectively. As a result, it can be concluded that a TRIM cross-linker allows constructing a polymer network that has a higher affinity to 5-FU and allows to imprint it more effectively than a network synthesized using the EGDMA cross-linker.

Table 1. Parameters of 5-FU adsorption by MIPs and NIPs.

Polymer	Langmuir			Freundlich		
	q_m (mg g^{-1})	K (L mg^{-1})	R^2	K$_f$ (mg g^{-1} (L mg^{-1})$^{1/n}$)	1/n	R^2
MIP$_{EGDMA}$	22.57 ± 1.96	0.285 ± 0.025	0.991	3.59 ± 0.32	0.62 ± 0.06	0.973
NIP$_{EGDMA}$	7.00 ± 0.64	0.142 ± 0.013	0.989	0.82 ± 0.08	0.60 ± 0.06	0.977
MIP$_{TRIM}$	37.30 ± 3.46	0.676 ± 0.064	0.997	9.72 ± 0.92	0.66 ± 0.06	0.937
NIP$_{TRIM}$	12.89 ± 1.63	0.088 ± 0.008	0.992	0.95 ± 0.09	0.73 ± 0.07	0.972

The following equations represent the Freundlich adsorption isotherm:

$$q_{eq} = K_f C_{eq}^{1/n} \tag{9}$$

$$\log q_{eq} = \log K_f + \frac{1}{n} \log C_{eq} \tag{10}$$

where K_f and n represent the Freundlich constants, C_{eq} (mg L^{-1}) is the equilibrium concentration of 5-FU, and q_{eq} (mg g^{-1}) is the amount of 5-FU adsorbed at the equilibrium concentration. Table 1 summarizes the values of K_f, $1/n$, and R^2 (correlation coefficients). The R^2 values obtained for MIP$_{EGDMA}$, NIP$_{EGDMA}$, and NIP$_{TRIM}$ are higher than 0.97, suggesting that the experimental data can be fitted using the Freundlich adsorption model. On the other hand, the R^2 values obtained for MIP$_{TRIM}$ are lower than 0.94, indicating that the Freundlich adsorption model should not be used to characterize the experimental results. The $1/n$ value calculated from the Freundlich adsorption model is considered a measure of adsorption intensity or surface heterogeneity. Basically, the closer the $1/n$ value to zero, the more heterogeneous the surface [49]. Moreover, if the value of $1/n$ is higher than one, then adsorption is considered cooperative [50]. The $1/n$ values obtained for all microparticles are similar and are in the 0.60–0.73 range. This result indicates that all materials' heterogeneity is similar and the adsorption of 5-FU on them follows a similar mechanism.

3.2. Adsorption Kinetics

Adsorption kinetics can be established by finding a relationship between the adsorption capacity of examined materials and the contact time with the adsorbate solution. For all synthesized microparticles, the plots of q_t versus t were obtained and are shown

in Figure S6. The experimental data were fitted using two adsorption kinetics models, the pseudo-first-order model given by Langergren and Svenska and the pseudo-second-order model based on the equilibrium adsorption. The following equation represents the pseudo-first-order model:

$$\log(q_e - q_t) = \log q_e - \frac{k_1}{2.303}t \tag{11}$$

where k_1 (h^{-1}) is the pseudo-first-order rate constant, q_e (mg g^{-1}) is the amount of 5-FU adsorbed at the equilibrium concentration, and q_t (mg g^{-1}) is the amount of 5-FU adsorbed at time t (h). The k_1 and R^2 values are presented in Table 2. The calculated R^2 values range between 0.979 and 0.993, which means that this model could be applied to characterize the kinetics of the adsorption of 5-FU on synthesized microparticles. However, after comparing these results with much higher R^2 values calculated for the pseudo-second-order kinetic model, it becomes clear that the pseudo-first-order kinetic model only partially fits the experimental data obtained for all microparticles.

Table 2. Kinetic parameters calculated for pseudo-first-order and pseudo-second-order models.

Polymer	Pseudo-First-Order Kinetic Model		Pseudo-Second-Order Kinetic Model	
	k_1 (h^{-1})	R^2	k_2 (g mg^{-1} h^{-1})	R^2
MIP_{EGDMA}	3.46 ± 0.31	0.987	1.03 ± 0.09	0.998
NIP_{EGDMA}	1.50 ± 0.14	0.979	1.00 ± 0.09	0.997
MIP_{TRIM}	2.47 ± 0.22	0.993	0.52 ± 0.05	0.999
NIP_{TRIM}	1.74 ± 0.15	0.980	1.73 ± 0.14	0.994

The following equation represents the pseudo-second-order kinetic model:

$$\frac{t}{q_t} = \frac{1}{k_2 q_e^2} + \frac{1}{q_e}t \tag{12}$$

where k_2 (g mg^{-1} h^{-1}) is the pseudo-second-order rate constant. The k_2 and R^2 values are presented in Table 2. The R^2 values calculated using this model are much higher than those obtained for the pseudo-second-order kinetic model and are in the 0.994–0.999 range. This result indicates that the pseudo-second-order kinetic model should be used to characterize the adsorption of 5-FU by synthesized microparticles. For both MIPs and NIPs, the k_2 values are quite similar and are within a level of 0.52–1.73, indicating that the kinetics of 5-FU adsorption for all materials is similar.

3.3. In Vitro Release Studies

Three buffer solutions of pH 2.2 (simulated gastric fluid), pH 5.0 (simulated tumor interstitium of tumor cells) [51,52], and pH 7.4 (simulated intravenous conditions) were used as release media for in vitro release studies of 5-FU from the structures of drug-loaded imprinted materials. The release profiles of 5-FU from these materials (Figures 3 and 4) clearly show entirely different properties of both MIPs depending on the cross-linker used. For each material and each examined pH value, a significant difference in the cumulative 5-FU release after statistical analysis has been noted ($p < 0.05$). For EGDMA-based MIPs (5-FU loading equal to 11.3 mg g^{-1}), the highest cumulative release (ca. 40%) was observed for pH 2.2, whereas a much lower release, equal to 20% and 12%, was observed for pH 5.0 and 7.4, respectively. This result clearly shows that the higher the pH, the lower the cumulative release. The observed behavior is probably caused by the higher protonation of carboxylic groups present in the polymer structure at lower pH values. This process disrupts interactions between carboxylic groups and drug molecules, leading to increased drug release. The release profiles obtained for the examined pH values are different depending on the buffer pH. For pH 5.0 and 7.4, a very high initial burst release

is observed, which means that after around 10 h, the release almost entirely reaches the final cumulative release values. On the other hand, the initial burst release at pH 2.2 is much lower, and after that, a steady release is observed, which lasts around 50 h, after which a final cumulative release value is reached. For TRIM-based MIPs (drug loading 24.2 mg g^{-1}), a completely different behavior is observed regarding the dependence of pH of the release medium on the cumulative 5-FU release. The highest cumulative release (ca. 86%) was observed for pH 7.4, whereas for pH 5.0 and 2.2, these values were lower, equal to 70% and 53%, respectively. This behavior, almost opposite to the results obtained for MIP$_{EGDMA}$, is presumably caused by the much higher hydrophobicity of the TRIM-based polymer network than the one observed for EGDMA-based polymers. As 5-FU is sparingly soluble in water, it possesses a relatively high affinity towards the hydrophilic environment, and therefore the hydrophobic TRIM-based polymer network does not form strong interactions with 5-FU drug molecules. As a result, at pH 7.4, the drug release from MIP$_{TRIM}$ has the highest value because, at this pH value, the polymer network's hydrophobicity is the highest. When the pH is lowered, the polymer's structure becomes protonated, increasing its hydrophilicity, leading to a lower 5-FU release from its structure. Moreover, a rapid release at pH 2.2 can be observed, which is probably connected with breaking interactions occurring between MIPs cavities and 5-FU. As a result, during release, the amount of 5-FU maintained in the MIP$_{TRIM}$ structure is physisorbed primarily on its structure due to the polymer's increased hydrophilicity. The higher hydrophobicity of the TRIM-based polymer network than the EGDMA-based network also explains the much higher cumulative percentage release of 5-FU for MIP$_{TRIM}$ than the one observed for MIP$_{EGDMA}$.

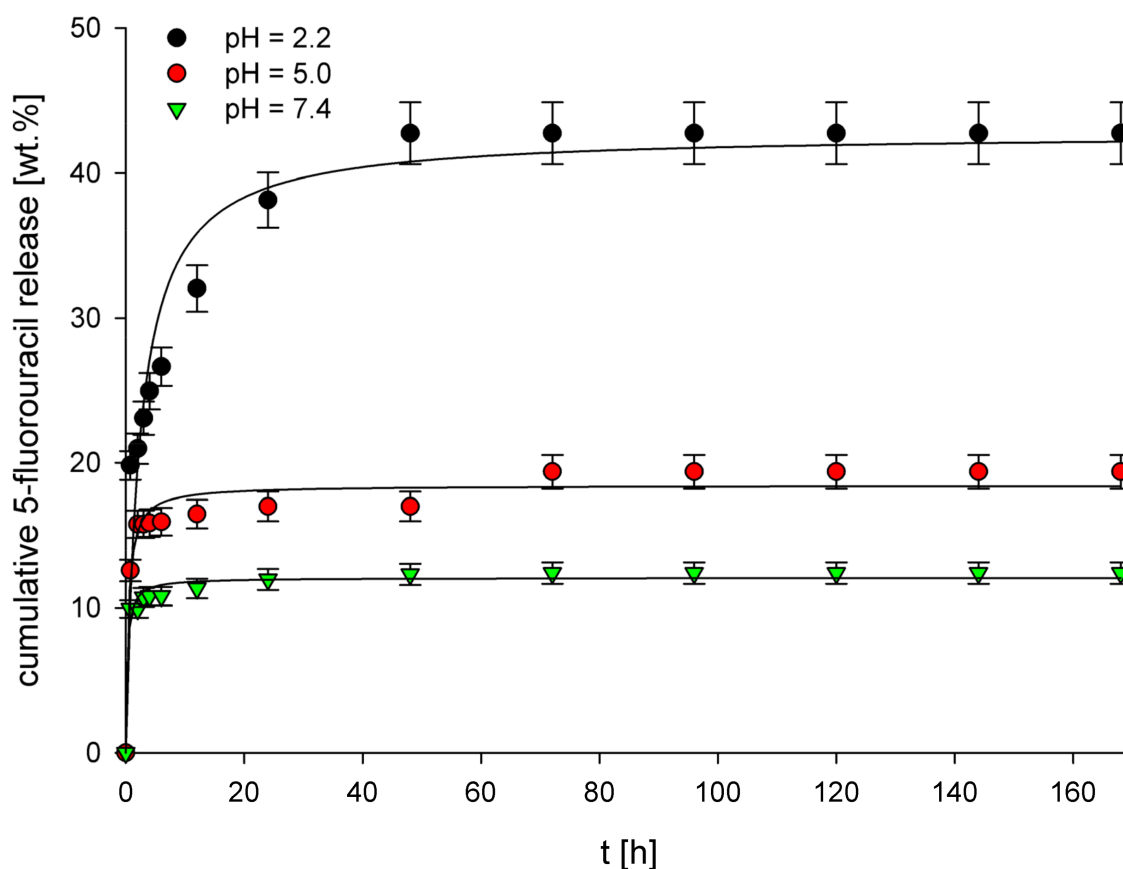**Figure 3.** Release profiles of 5-FU from MIP$_{EGDMA}$ at pH 2.2, 5.0, and 7.4.
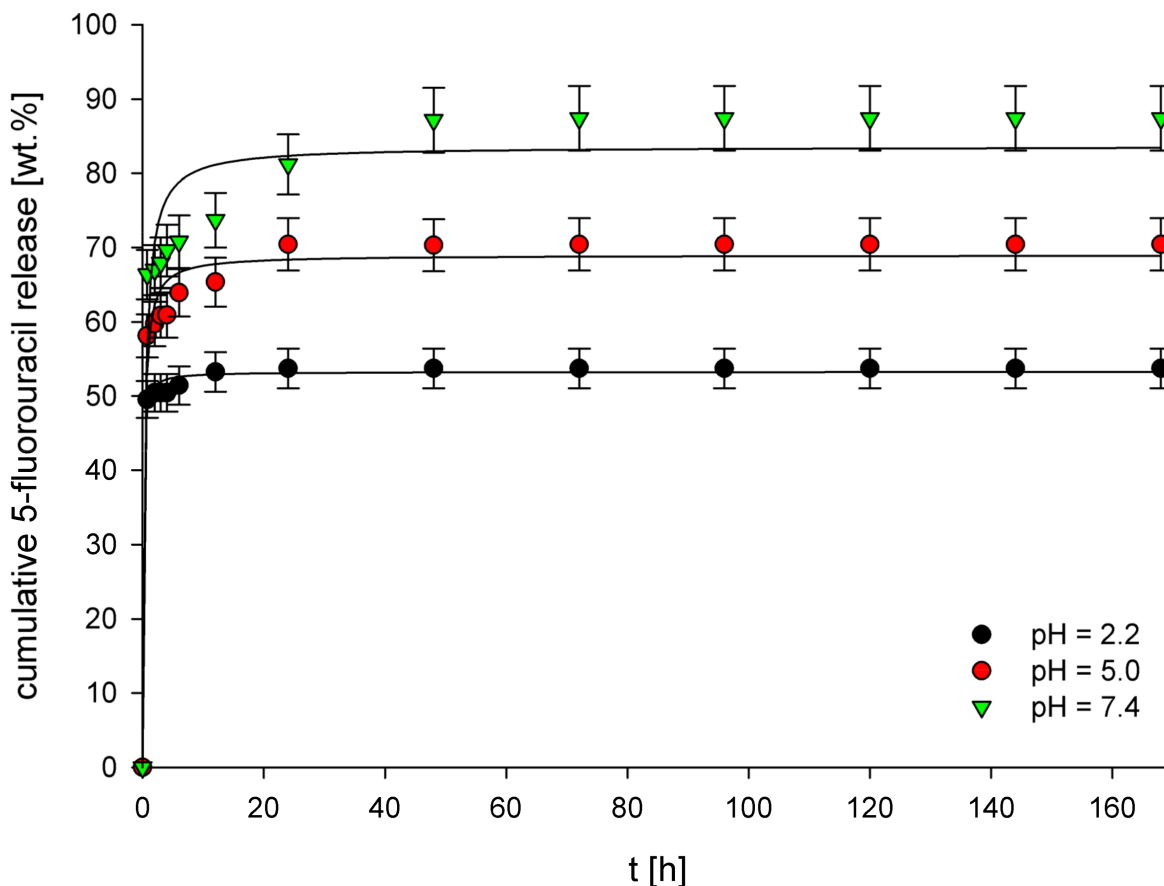
Figure 4. Release profiles of 5-FU from MIP$_{TRIM}$ at pH 2.2, 5.0, and 7.4.

Several mathematical models were used to fit the experimental data obtained from the 5-FU release from MIP$_{EGDMA}$ and MIP$_{TRIM}$. The release profiles were fitted with zero-order, first-order, Higuchi, Hixson–Crowell, and Korsmeyer–Peppas release models. The values of corresponding release constants (k), correlation coefficients (R^2), and the diffusion exponents (n) are presented in Table 3. For almost all pH values and both imprinted materials, the highest R^2 values were calculated for the Korsmeyer–Peppas release model, which indicates that the experimental data is best fitted with this model. The only exception is the release of 5-FU from MIP$_{TRIM}$ at pH 5.0, for which a higher R^2 value was obtained for the Higuchi model ($R^2 = 0.977$) compared to the Korsmeyer–Peppas model ($R^2 = 0.956$). However, the differences in the R^2 values are not significant; therefore, it can be concluded that the experimental data is nicely fitted with both of these models. These results indicate that the release mechanism of 5-FU from both MIPs at all examined pH values is similar. Moreover, for all MIPs at all examined pH values, the diffusion exponent value in the Korsmeyer–Peppas model was lower than 0.45, indicating a Fickian diffusion-controlled release mechanism.

Table 3. Release kinetic data of 5-FU from MIP_{EGDMA} and MIP_{TRIM}.

Polymer	pH	Zero-Order		First-Order		Higuchi		Hixson–Crowell		Korsmeyer–Peppas		
		k_0 (h^{-1})	R^2	k_1 (h^{-1})	R^2	k_H ($h^{-1/2}$)	R^2	k_{HC} ($h^{-1/3}$)	R^2	k_{KP} (h^{-n})	n	R^2
MIP_{EGDMA}	2.2	0.106 ± 0.093	0.621	$1.63 \times 10^{-3} \pm 0.14 \times 10^{-3}$	0.634	1.73 ± 0.15	0.791	$2.19 \times 10^{-3} \pm 0.20 \times 10^{-3}$	0.630	20.7 ± 1.8	0.16 ± 0.2	0.900
	5.0	0.110 ± 0.009	0.405	$1.30 \times 10^{-3} \pm 0.11 \times 10^{-3}$	0.413	0.77 ± 0.07	0.555	$1.91 \times 10^{-3} \pm 0.17 \times 10^{-3}$	0.410	13.9 ± 1.2	0.07 ± 0.01	0.726
	7.4	0.047 ± 0.004	0.784	$0.53 \times 10^{-3} \pm 0.05 \times 10^{-3}$	0.787	0.40 ± 0.04	0.910	$0.79 \times 10^{-3} \pm 0.07 \times 10^{-3}$	0.786	9.9 ± 0.9	0.06 ± 0.01	0.944
MIP_{TRIM}	2.2	0.085 ± 0.008	0.670	$1.77 \times 10^{-3} \pm 0.14 \times 10^{-3}$	0.674	0.70 ± 0.07	0.803	$1.93 \times 10^{-3} \pm 0.16 \times 10^{-3}$	0.661	49.3 ± 4.7	0.03 ± 0.01	0.896
	5.0	0.494 ± 0.42	0.944	$6.82 \times 10^{-3} \pm 0.61 \times 10^{-3}$	0.783	3.01 ± 0.28	0.977	$1.46 \times 10^{-2} \pm 0.11 \times 10^{-2}$	0.966	56.5 ± 5.2	0.06 ± 0.01	0.956
	7.4	0.130 ± 0.011	0.705	$6.40 \times 10^{-3} \pm 0.59 \times 10^{-3}$	0.737	1.96 ± 0.16	0.867	$5.78 \times 10^{-3} \pm 0.53 \times 10^{-3}$	0.728	64.8 ± 6.2	0.06 ± 0.01	0.947

3.4. In Vitro Cell Viability

Cytotoxicity against U87 MG, HeLa, KB, A-549, and MCF-7 cancer cell lines, and HDF normal cell lines, was examined for drug-loaded and drug-unloaded MIPs and pure 5-FU. Table 4 summarizes the IC_{50} values. Both drug-loaded MIPs present very high cytotoxicity against cancer cell lines, contrary to the result obtained for drug-unloaded MIPs. The results clearly show that drug-loaded MIP_{TRIM} shows almost identical cytotoxicity against HeLa cancer cell lines as pure 5-FU. In contrast, its cytotoxicity against normal HDF cell lines is nearly three times lower than that measured for 5-FU. As a result, it can be concluded that MIP_{TRIM} can be a good candidate as a DDS for 5-FU because it allows maintaining high cytotoxicity against HeLa cell lines while lowering the cytotoxicity against healthy cells.

Table 4. The IC_{50} values ($\mu g\ mL^{-1}$) obtained for drug-loaded and unloaded MIPs and pure 5-FU. Standard deviations are presented in brackets.

Material	U87 MG	HeLa	KB	A-549	MCF-7	HDF
unloaded MIP_{EGDMA}	62.13 (0.11)	67.02 (0.49)	67.39 (0.07)	71.08 (0.73)	63.35 (0.19)	98.19 (0.51)
unloaded MIP_{TRIM}	81.12 (0.04)	69.02 (0.31)	81.01 (1.04)	77.82 (0.59)	81.93 (0.94)	102.02 (0.87)
loaded MIP_{EGDMA}	0.38 (0.07)	1.02 (0.11)	0.41 (0.16)	0.31 (0.91)	0.19 (0.01)	0.44 (0.49)
loaded MIP_{TRIM}	0.50 (0.04)	0.16 (0.01)	0.21 (0.17)	0.26 (0.19)	0.22 (0.01)	1.94 (0.55)
5-FU	0.07 (0.01)	0.16 (0.13)	0.03 (0.01)	0.08 (0.03)	0.08 (0.07)	0.71 (0.05)

4. Conclusions

We have shown that microparticles imprinted with 5-FU can be applied for the prolonged release of this drug. The microparticles synthesized using the TRIM cross-linker showed higher adsorption properties towards 5-FU than those synthesized using EGDMA. The experiments proved that prolonged drug release could last up to 50 h when an EGDMA cross-linker is used. The calculated highest cumulative release was highly dependent on the cross-linker applied during the synthesis. For EGDMA-based MIPs, the highest cumulative release was observed at pH 2.2, lower at pH 5.0, and the lowest at pH 7.4. Opposite results were obtained for TRIM-based MIPs, as the highest cumulative release was obtained for pH 7.4 and the lowest for pH 2.2. Moreover, the overall cumulative release was much higher for TRIM-based than EGDMA-based MIPs. The 5-FU release from all examined materials at all pH values was well fitted with the Korsmeyer–Peppas model. The IC_{50} values proved that drug-loaded MIP_{TRIM} possesses high cytotoxic activity against cancer cell lines, while lowering the toxicity towards normal HDF cell lines. Therefore, it has been proven that the selection of a cross-linker has a significant impact on the final properties of microparticles and has to be considered during the design of materials used for drug delivery.

Supplementary Materials: The following supporting information can be downloaded at: https://www.mdpi.com/article/10.3390/polym14051027/s1, Figure S1: Chemical structures of 5- fluorouracil, functional monomers, and cross-linkers. Figure S2: FT-IR spectra of loaded MIP_{EGDMA}, unloaded MIP_{EGDMA}, and NIP_{EGDMA}. Figure S3: FT-IR spectra of loaded MIP_{TRIM}, unloaded

MIP$_{TRIM}$, and NIP$_{TRIM}$. Figure S4: Results of thermogravimetric analysis for NIP$_{EGDMA}$, unloaded MIP$_{EGDMA}$, and loaded MIP$_{EGDMA}$. Figure S5: Results of thermogravimetric analysis for NIP$_{TRIM}$, unloaded MIP$_{TRIM}$, and loaded MIP$_{TRIM}$. Figure S6: The relationship between q$_t$ and t obtained for MIP$_{EGDMA}$, NIP$_{EGDMA}$, MIP$_{TRIM}$, and NIP$_{TRIM}$ during adsorption kinetics experiments.

Author Contributions: Conceptualization, M.C.; materials' synthesis and characterization, M.C. and A.L.; adsorption experiments, M.C. and T.N.; release experiments, J.K.; interpretation of the adsorption and release data, M.C. and J.K.; cytotoxicity assays and data interpretation, P.R.; writing—original draft preparation, M.C.; writing—review and editing, M.C.; supervision, M.C.; funding acquisition, M.C. All authors have read and agreed to the published version of the manuscript.

Institutional Review Board Statement: Not applicable.

Informed Consent Statement: Not applicable.

Data Availability Statement: The additional data that support the findings of this study are available from the corresponding author upon request.

Conflicts of Interest: The authors declare no conflict of interest. The funders had no role in the design of the study; in the collection, analyses, or interpretation of data; in the writing of the manuscript, or in the decision to publish the results.

References

1. Allen, T.M.; Cullis, P.R. Drug Delivery Systems: Entering the Mainstream. *Science* **2004**, *303*, 1818–1822. [CrossRef]
2. Mura, S.; Nicolas, J.; Couvreur, P. Stimuli-responsive nanocarriers for drug delivery. *Nat. Mater.* **2013**, *12*, 991–1003. [CrossRef] [PubMed]
3. Kataoka, K.; Harada, A.; Nagasaki, Y. Block copolymer micelles for drug delivery: Design, characterization and biological significance. *Adv. Drug Deliv. Rev.* **2001**, *47*, 113–131. [CrossRef]
4. Abdou, E.M.; Fayed, M.A.A.; Helal, D.; Ahmed, K.A. Assessment of the hepatoprotective effect of developed lipid-polymer hybrid nanoparticles (LPHNPs) encapsulating naturally extracted β-Sitosterol against CCl$_4$ induced hepatotoxicity in rats. *Sci. Rep.* **2019**, *9*, 19779. [CrossRef] [PubMed]
5. Iachetta, G.; Falanga, A.; Molino, Y.; Masse, M.; Jabès, F.; Mechioukhi, Y.; Laforgia, V.; Khrestchatisky, M.; Galdiero, S.; Valiante, S. gH625-liposomes as tool for pituitary adenylate cyclase-activating polypeptide brain delivery. *Sci. Rep.* **2019**, *9*, 9183. [CrossRef]
6. Wei, Y.; Huang, Y.-H.; Cheng, K.-C.; Song, Y.-L. Investigations of the Influences of Processing Conditions on the Properties of Spray Dried Chitosan-Tripolyphosphate Particles loaded with Theophylline. *Sci. Rep.* **2020**, *10*, 1155. [CrossRef]
7. Babu, A.; Amreddy, N.; Muralidharan, R.; Pathuri, G.; Gali, H.; Chen, A.; Zhao, Y.D.; Munshi, A.; Ramesh, R. Chemodrug delivery using integrin-targeted PLGA-Chitosan nanoparticle for lung cancer therapy. *Sci. Rep.* **2017**, *7*, 14674. [CrossRef]
8. Zhang, D.-X.; Yoshikawa, C.; Welch, N.G.; Pasic, P.; Thissen, H.; Voelcker, N.H. Spatially Controlled Surface Modification of Porous Silicon for Sustained Drug Delivery Applications. *Sci. Rep.* **2019**, *9*, 1367. [CrossRef]
9. Cai, D.; Liu, L.; Han, C.; Ma, X.; Qian, J.; Zhou, J.; Zhu, W. Cancer cell membrane-coated mesoporous silica loaded with superparamagnetic ferroferric oxide and Paclitaxel for the combination of Chemo/Magnetocaloric therapy on MDA-MB-231 cells. *Sci. Rep.* **2019**, *9*, 14475. [CrossRef]
10. Amolegbe, S.A.; Hirano, Y.; Adebayo, J.O.; Ademowo, O.G.; Balogun, E.A.; Obaleye, J.A.; Krettli, A.U.; Yu, C.; Hayami, S. Mesoporous silica nanocarriers encapsulated antimalarials with high therapeutic performance. *Sci. Rep.* **2018**, *8*, 3078. [CrossRef]
11. Cheng, C.; Gao, Y.; Song, W.; Zhao, Q.; Zhang, H.; Zhang, H. Halloysite nanotube-based H2O2-responsive drug delivery system with a turn on effect on fluorescence for real-time monitoring. *Chem. Eng. J.* **2020**, *380*, 122474. [CrossRef]
12. Sharif, S.; Abbas, G.; Hanif, M.; Bernkop-Schnürch, A.; Jalil, A.; Yaqoob, M. Mucoadhesive micro-composites: Chitosan coated halloysite nanotubes for sustained drug delivery. *Colloids Surf. B* **2019**, *184*, 110527. [CrossRef]
13. Nagiah, N.; Murdock, C.J.; Bhattacharjee, M.; Nair, L.; Laurencin, C.T. Development of Tripolymeric Triaxial Electrospun Fibrous Matrices for Dual Drug Delivery Applications. *Sci. Rep.* **2020**, *10*, 609. [CrossRef]
14. Fortuni, B.; Inose, T.; Ricci, M.; Fujita, Y.; Van Zundert, I.; Masuhara, A.; Fron, E.; Mizuno, H.; Latterini, L.; Rocha, S.; et al. Polymeric Engineering of Nanoparticles for Highly Efficient Multifunctional Drug Delivery Systems. *Sci. Rep.* **2019**, *9*, 2666. [CrossRef]
15. Kharaghani, D.; Gitigard, P.; Ohtani, H.; Kim, K.O.; Ullah, S.; Saito, Y.; Khan, M.Q.; Kim, I.S. Design and characterization of dual drug delivery based on in-situ assembled PVA/PAN core-shell nanofibers for wound dressing application. *Sci. Rep.* **2019**, *9*, 12640. [CrossRef]
16. Gao, J.; Dutta, K.; Zhuang, J.; Thayumanavan, S. Cellular- and Subcellular-Targeted Delivery Using a Simple All-in-One Polymeric Nanoassembly. *Angew. Chem. Int. Ed.* **2020**, *59*, 23466–23470. [CrossRef]

17. Li, Y.; Maciel, D.; Rodrigues, J.; Shi, X.; Tomás, H. Biodegradable Polymer Nanogels for Drug/Nucleic Acid Delivery. *Chem. Rev.* **2015**, *115*, 8564–8608. [CrossRef]

18. Gao, J.; Wu, P.; Fernandez, A.; Zhuang, J.; Thayumanavan, S. Cellular AND Gates: Synergistic Recognition to Boost Selective Uptake of Polymeric Nanoassemblies. *Angew. Chem. Int. Ed.* **2020**, *59*, 10456–10460. [CrossRef]

19. Molina, M.; Asadian-Birjand, M.; Balach, J.; Bergueiro, J.; Miceli, E.; Calderón, M. Stimuli-responsive nanogel composites and their application in nanomedicine. *Chem. Soc. Rev.* **2015**, *44*, 6161–6186. [CrossRef]

20. Kokil, G.R.; Veedu, R.N.; Le, B.T.; Ramm, G.A.; Parekh, H.S. Self-assembling asymmetric peptide-dendrimer micelles—a platform for effective and versatile in vitro nucleic acid delivery. *Sci. Rep.* **2018**, *8*, 4832. [CrossRef]

21. Zhang, H.; Ma, Y.; Xie, Y.; An, Y.; Huang, Y.; Zhu, Z.; Yang, C.J. A Controllable Aptamer-Based Self-Assembled DNA Dendrimer for High Affinity Targeting, Bioimaging and Drug Delivery. *Sci. Rep.* **2015**, *5*, 10099. [CrossRef]

22. Smoluch, M.; Ceglowski, M.; Kurczewska, J.; Babij, M.; Gotszalk, T.; Silberring, J.; Schroeder, G. Molecular Scavengers as Carriers of Analytes for Mass Spectrometry Identification. *Anal. Chem.* **2014**, *86*, 11226–11229. [CrossRef]

23. Narkiewicz, U.; Pełech, I.; Podsiadły, M.; Cegłowski, M.; Schroeder, G.; Kurczewska, J. Preparation and characterization of magnetic carbon nanomaterials bearing APTS–silica on their surface. *J. Mater. Sci.* **2010**, *45*, 1100–1106. [CrossRef]

24. Sellergren, B.; Allender, C.J. Molecularly imprinted polymers: A bridge to advanced drug delivery. *Adv. Drug Deliv. Rev.* **2005**, *57*, 1733–1741. [CrossRef]

25. Mokhtari, P.; Ghaedi, M. Water compatible molecularly imprinted polymer for controlled release of riboflavin as drug delivery system. *Eur. Polym. J.* **2019**, *118*, 614–618. [CrossRef]

26. Tuwahatu, C.A.; Yeung, C.C.; Lam, Y.W.; Roy, V.A.L. The molecularly imprinted polymer essentials: Curation of anticancer, ophthalmic, and projected gene therapy drug delivery systems. *J. Control. Release* **2018**, *287*, 24–34. [CrossRef]

27. Zhang, Z.; Cao, X.; Zhang, Z.; Yin, J.; Wang, D.; Xu, Y.; Zheng, W.; Li, X.; Zhang, Q.; Liu, L. Synthesis of dummy-template molecularly imprinted polymer adsorbents for solid phase extraction of aminoglycosides antibiotics from environmental water samples. *Talanta* **2020**, *208*, 120385. [CrossRef]

28. Tamayo, F.G.; Turiel, E.; Martín-Esteban, A. Molecularly imprinted polymers for solid-phase extraction and solid-phase microextraction: Recent developments and future trends. *J. Chromatogr. A* **2007**, *1152*, 32–40. [CrossRef]

29. Andersson, L.I. Molecular imprinting for drug bioanalysis: A review on the application of imprinted polymers to solid-phase extraction and binding assay. *J. Chromatogr. B* **2000**, *739*, 163–173. [CrossRef]

30. Whitcombe, M.J.; Chianella, I.; Larcombe, L.; Piletsky, S.A.; Noble, J.; Porter, R.; Horgan, A. The rational development of molecularly imprinted polymer-based sensors for protein detection. *Chem. Soc. Rev.* **2011**, *40*, 1547–1571. [CrossRef]

31. Kidakova, A.; Boroznjak, R.; Reut, J.; Öpik, A.; Saarma, M.; Syritski, V. Molecularly imprinted polymer-based SAW sensor for label-free detection of cerebral dopamine neurotrophic factor protein. *Sens. Actuat. B-Chem.* **2020**, *308*, 127708. [CrossRef]

32. Zhao, X.; He, Y.; Wang, Y.; Wang, S.; Wang, J. Hollow molecularly imprinted polymer based quartz crystal microbalance sensor for rapid detection of methimazole in food samples. *Food Chem.* **2020**, *309*, 125787. [CrossRef] [PubMed]

33. Hashemi-Moghaddam, H.; Kazemi-Bagsangani, S.; Jamili, M.; Zavareh, S. Evaluation of magnetic nanoparticles coated by 5-fluorouracil imprinted polymer for controlled drug delivery in mouse breast cancer model. *Int. J. Pharm.* **2016**, *497*, 228–238. [CrossRef] [PubMed]

34. Li, L.; Chen, L.; Zhang, H.; Yang, Y.; Liu, X.; Chen, Y. Temperature and magnetism bi-responsive molecularly imprinted polymers: Preparation, adsorption mechanism and properties as drug delivery system for sustained release of 5-fluorouracil. *Mater. Sci. Eng. C* **2016**, *61*, 158–168. [CrossRef]

35. Parisi, O.I.; Morelli, C.; Puoci, F.; Saturnino, C.; Caruso, A.; Sisci, D.; Trombino, G.E.; Picci, N.; Sinicropi, M.S. Magnetic molecularly imprinted polymers (MMIPs) for carbazole derivative release in targeted cancer therapy. *J. Mater. Chem. B* **2014**, *2*, 6619–6625. [CrossRef]

36. Norell, M.C.; Andersson, H.S.; Nicholls, I.A. Theophylline molecularly imprinted polymer dissociation kinetics: A novel sustained release drug dosage mechanism. *J. Mol. Recognit.* **1998**, *11*, 98–102. [CrossRef]

37. Cegłowski, M.; Kurczewska, J.; Ruszkowski, P.; Liberska, J.; Schroeder, G. The influence of cross-linking agent onto adsorption properties, release behavior and cytotoxicity of doxorubicin-imprinted microparticles. *Colloids Surf. B* **2019**, *182*, 110379. [CrossRef]

38. Cegłowski, M.; Kurczewska, J.; Ruszkowski, P.; Schroeder, G. Application of paclitaxel-imprinted microparticles obtained using two different cross-linkers for prolonged drug delivery. *Eur. Polym. J.* **2019**, *118*, 328–336. [CrossRef]

39. Jia, C.; Zhang, M.; Zhang, Y.; Ma, Z.-B.; Xiao, N.-N.; He, X.-W.; Li, W.-Y.; Zhang, Y.-K. Preparation of Dual-Template Epitope Imprinted Polymers for Targeted Fluorescence Imaging and Targeted Drug Delivery to Pancreatic Cancer BxPC-3 Cells. *ACS Appl. Mater. Interfaces* **2019**, *11*, 32431–32440. [CrossRef]

40. Hashemi-Moghaddam, H.; Zavareh, S.; Karimpour, S.; Madanchi, H. Evaluation of molecularly imprinted polymer based on HER2 epitope for targeted drug delivery in ovarian cancer mouse model. *React. Funct. Polym.* **2017**, *121*, 82–90. [CrossRef]

41. Marcelo, G.; Ferreira, I.C.; Viveiros, R.; Casimiro, T. Development of itaconic acid-based molecular imprinted polymers using supercritical fluid technology for pH-triggered drug delivery. *Int. J. Pharm.* **2018**, *542*, 125–131. [CrossRef]

42. Arias, J.L. Novel strategies to improve the anticancer action of 5-fluorouracil by using drug delivery systems. *Molecules* **2008**, *13*, 2340–2369. [CrossRef]

43. Cegłowski, M.; Jerca, V.V.; Jerca, F.A.; Hoogenboom, R. Reduction-Responsive Molecularly Imprinted Poly(2-isopropenyl-2-oxazoline) for Controlled Release of Anticancer Agents. *Pharmaceutics* **2020**, *12*, 506. [CrossRef]

44. Lengyel, M.; Kállai-Szabó, N.; Antal, V.; Laki, A.J.; Antal, I. Microparticles, Microspheres, and Microcapsules for Advanced Drug Delivery. *Sci. Pharm.* **2019**, *87*, 20. [CrossRef]

45. Bettencourt, A.; Almeida, A.J. Poly(methyl methacrylate) particulate carriers in drug delivery. *J. Microencapsul.* **2012**, *29*, 353–367. [CrossRef]

46. Farzaneh, S.; Asadi, E.; Abdouss, M.; Barghi-Lish, A.; Azodi-Deilami, S.; Khonakdar, H.A.; Gharghabi, M. Molecularly imprinted polymer nanoparticles for olanzapine recognition: Application for solid phase extraction and sustained release. *RSC Adv.* **2015**, *5*, 9154–9166. [CrossRef]

47. Javanbakht, M.; Attaran, A.M.; Namjumanesh, M.H.; Esfandyari-Manesh, M.; Akbari-adergani, B. Solid-phase extraction of tramadol from plasma and urine samples using a novel water-compatible molecularly imprinted polymer. *J. Chromatogr. B* **2010**, *878*, 1700–1706. [CrossRef]

48. Gupta, A.; Tiwari, G.; Tiwari, R.; Srivastava, R.; Rai, A.K. Enteric coated HPMC capsules plugged with 5-FU loaded microsponges: A potential approach for treatment of colon cancer. *Braz. J. Pharm. Sci.* **2015**, *51*, 591–606. [CrossRef]

49. Haghseresht, F.; Lu, G.Q. Adsorption Characteristics of Phenolic Compounds onto Coal-Reject-Derived Adsorbents. *Energy Fuels* **1998**, *12*, 1100–1107. [CrossRef]

50. Fytianos, K.; Voudrias, E.; Kokkalis, E. Sorption–desorption behaviour of 2,4-dichlorophenol by marine sediments. *Chemosphere* **2000**, *40*, 3–6. [CrossRef]

51. Dand, N.; Patel, P.; Ayre, A.; Kadam, V. Polymeric micelles as a drug carrier for tumor targeting. *Chron. Young Sci.* **2013**, *4*, 94–101. [CrossRef]

52. Bai, J.; Zhang, Y.; Chen, L.; Yan, H.; Zhang, C.; Liu, L.; Xu, X. Synthesis and characterization of paclitaxel-imprinted microparticles for controlled release of an anticancer drug. *Mater. Sci. Eng. C* **2018**, *92*, 338–348. [CrossRef]